Materials and Design 87 (2015) 996–1002

Contents lists available at ScienceDirect

Materials and Design

journal homepage: www.elsevier.com/locate/jmad

Preparation of Al–Si alloys by a rapid solidification and powder metallurgy route

Zhiyong Cai, Chun Zhang, Richu Wang *, Chaoqun Peng, Ke Qiu, Yan Feng

School of Materials Science and Engineering, Central South University, Changsha 410083, China

ARTICLE INFO

Article history:
Received 15 July 2015
Received in revised form 18 August 2015
Accepted 20 August 2015
Available online 28 August 2015

Keywords:
Aluminum silicon alloy
Powder metallurgy
Microstructure
Mechanical property
Physical property

ABSTRACT

The Al–(22–50 wt.%) Si alloys are prepared by hot pressing of gas atomized Al–Si alloy powder. The microstructures, mechanical properties, physical properties, and fracture surfaces of the alloys are characterized as a function of the Si content. All the alloys are well densified with pore-free microstructure and homogeneously dispersed Si phase that is refined in size and has smooth surface. The mechanical properties of the alloys are improved gradually with increasing Si content, especially the bending strength. However, both the coefficient of thermal expansion (CTE) and thermal conductivity of the alloy decrease at the same time. The average CTE and thermal conductivity of the Al–Si alloys are 18.7–11.3 10^{-6}/K and 184–145 W/m K, respectively, indicating excellent performance of these alloys. Theoretical models are used to predict the CTE and thermal conductivity of the alloys. Moreover, the thermal boundary resistance at the interface of Al and Si is also calculated.

1. Introduction

For decades, the continuous progress of microelectronic systems with high calculating speed and miniaturization leads to the rapid increase of functional density. As a result, efficient heat management is demanded in microelectronics to prevent overheating induced performance degradation or even device failures [1,2]. Therefore, developing materials with high thermal conductivity is imperative for heat sinks and heat spreaders. Additionally, compatible coefficient of thermal expansion (CTE) matching with those of semiconductor materials or ceramic substrates is also demanded to minimize the thermal stress and enhance the reliability of electronic components [3–5].

Particles reinforced Al matrix composites (AMCs) usually exhibit superior mechanical and thermo-physical performances due to the combination of the excellent properties of Al matrix and reinforcement [6,7]. Al–Si alloys, also called Sip reinforced AMCs have received increasing interest in the application of electronic packaging for thermal management and high performance engines because Si is widely available, low-cost, and environmental-friendly [8–11]. Meanwhile, the good machinability of Al–Si alloys compared with the Al–SiCp composites also makes them attractive for precision machined components [12,13]. According to the Al–Si binary phase diagram, the solubility of Si in Al and the absence of interfacial reactions at high temperatures promote the consolidation process of the Al–Si alloys [12].

Al–Si alloys have been fabricated by various techniques, e.g., pressure infiltration [12,14], squeeze casting [15], spray deposition [9,16], semi-solid process [17], and powder metallurgy (PM) [8,18]. Although infiltration process can obtain the Al–Si alloys with high Si content (>60 wt.%), some closed pores cannot be completely filled and will exist in the alloys, and the ratio of Si to Al is hard to be strictly controlled [1]. Spray deposition technology is a form of rapid solidification, which can effectively suppress the Si phase in size and morphology. However, the high cost and complex processing parameters, such as melt flow rate, melt atomization, and deposition rate, restrict the wide applications of spray deposition. Additionally, billets have to be further machined and densified in order to exclude the residual porosity [1,12]. The most effective and relatively simple route may be the PM technique via cold pressing of mixed or pre-alloyed powder following pressure or pressureless sintering. Moreover, the PM technique is valuable to add the reinforcement with a wide range of amount [11,19]. In this respect, the hot pressing process of AMCs is favorable because it involves comparatively high applied pressure, low sintering temperature (about 500–650 °C, depending on matrix alloy composition), near-full density, and high productivity [13,20,21].

In this work, Al–Si alloys containing 22–50 wt.% Si were fabricated by hot pressing of gas atomized Al–Si alloy powder. This work aims at providing a contribution to clarify the effect of Si content on the microstructure and thermo-mechanical properties of Al–Si alloys. Therefore, the effect of Si content on the microstructure characteristics, mechanical properties, physical properties, and fracture mechanism of the alloys were evaluated.

2. Experimental procedure

Polycrystalline pure Si (99.9 wt.%) with the contents of 22, 27, 42, and 50 wt.% were inductively melted with pure Al (99.9 wt.%) at 900,

* Corresponding author.
E-mail address: rcwcsu@163.com (R. Wang).

http://dx.doi.org/10.1016/j.matdes.2015.08.106
0264-1275/

950, 1150, and 1250 °C, respectively. The molted alloy was poured into a pre-heated graphite tundish with an inner diameter of 2.5–3.5 mm at 0.9 MPa. During atomization, a fine dispersion of droplets was formed when the molten Al–Si alloy was impacted by a high energy nitrogen gas. Irregular Al–Si alloy powder was obtained by gas atomization with oxygen content less than 800 ppm. The as-atomized powder was mechanically sieved to less than 74 μm (200 mesh). The average microhardness of the powder increases from 107 HV to 193 HV with increasing Si content. The powder was subjected to double action axial compaction in a steel die with an inner diameter of 50 mm under 400 MPa for 2 min. The relative densities of compacts are in the range of 75–80%, depending on the Si content. Then the green billets were sintered by hot pressing in a graphite die. The inner walls of die were coated with BN slurry. The furnace was heated to 400 °C and held for 30 min at a pressure of 20 MPa in order to degas the powder compacts. The maximum uniaxial pressure was 45 MPa. The selected sintering temperature and holding time were 565 °C and 60 min, respectively. The heating rate was 15 °C/min. The temperature during hot pressing was monitored by a thermocouple inserted to the die. The indicated temperature fluctuated by ±2 °C around the set value. The pressure on the specimens was not released until cooled down to 200 °C. After sintering, the hot pressed specimens were cooled in furnace to the room temperature. Hot pressed specimens were in the form of discs with a diameter of 50 and a thickness of about 10 mm.

The oxygen contents of Al–Si alloy powder and hot pressed samples were detected with a TCH600 analyzer. Specimens used for microstructural observations were prepared by standard metallurgical methods, i.e., grinding on SiC abrasive papers and polishing with 1 μm diamond paste, followed by etching with Keller's reagent (a solution of 1 vol.% HF–1.5 vol.% HCl–2.5 vol.% HNO_3–95 vol.% H_2O). The microstructures of alloys and morphologies of Si reinforcement were observed using a scanning electron microscope (SEM, FEI QUANTA-200). Image analysis was carried out to measure the average size of Si phase. X-ray diffraction (XRD) analysis was carried out with a Rigaku D/Max2500VB+ diffractometer using Cu Kα radiation at a scan step of 0.08 (°)/s. The fractographic examinations were carried out on the broken tensile specimens using SEM.

The Vickers microhardness measurements were carried out on the matrix of powder, and performed on a Vicker scale using a diamond indenter with 0.25 kN for 15 s (HDX-1000). Cylindrical disc specimens with dimensions of 10 mm in diameter and 3 mm in thickness were cut from the hot pressed samples for measuring the thermal conductivity, which was calculated as the product of density, thermal diffusivity and specific heat. Thermal diffusivity and specific heat were measured by laser flash method and calorimetric techniques (NETZSCH LFA427/3/G), respectively. The densities of the alloys were measured using the Archimedes method. CTE measurements were carried out on a NETZSCH DIL 402C dilatometer. The specimens with a diameter of 3 mm and a length of 25 mm were heated from room temperature to 400 °C with a heating and cooling rate of 5 °C/min. The Brinell hardness measurements were performed on the cross-section of the hot pressed samples. Both tensile and three point bending tests were performed at room temperature with an initial strain rate of 0.5 mm/min using an Instron testing machine (MTS 850). Tensile specimens with dog bone-shaped circular (a gauge diameter of 5 mm and gauge length of 10 mm) and bending specimens with square shape (thickness, width, and length of 3, 10, and 50 mm, respectively) were used. Three or more parallel tests were conducted to ensure good reproducibility of the data.

3. Results and discussion

3.1. Microstructure characteristics

Fig. 1 shows the microstructures of the hot pressed Al–Si alloys. It can be seen that the Si particles are refined in size and distribute homogeneously in the Al matrix as a result of using Al–Si pre-alloyed powder as raw material. The Al–Si eutectic phase is absent in these samples. For Al–22 wt.% Si and Al–27 wt.% Si alloy, as seen in Fig. 1a and b, respectively, most of the Si particles are separated randomly in the matrix. The Si particles are more interconnected with each other as the Si content increases (Fig. 1c and d). This phenomenon is different to the conventional AMCs reinforced with ceramic particles, such as Al–SiCp composites [22,23]. Additionally, the microstructures of Al–42 wt.% Si and Al–50 wt.% Si samples show a semi-continuous network of globular Si phase dispersed in the Al matrix. The size of Si particles in the Al–50 wt.% Si alloy is 5–18 μm, which is comparable to that prepared by spray deposition followed by hot isostatic pressing (HIP) [9]. The globular Si phase is surrounded by an interpenetrating Al matrix. The presence of semi-continuous Si phase is valuable to obtain alloys with low CTE because the thermal expansion of Al matrix is more efficiently inhibited. Moreover, the Si phase with globular morphology and smooth surface can improve the mechanical properties and thermal cycling resistance because cracks usually initiate at the phase with sharp corners [24,25]. Despite the semi-continuous Si phase, the interpenetrating Al matrix exhibits no closed region. It is reported that a continuous matrix is necessary for the alloys with excellent thermal properties because the thermal conductivity of Al is higher than that of Si [8].

Fig. 2 shows the XRD patterns of the hot pressed Al–Si alloys with various Si contents. All diffraction peaks are attributed to the α-Al or β-Si phase, and no additional intermetallic or compound can be observed. Therefore, no detrimental reaction occurs during the fabrication process. This result indicates that no thermal treatment will occur during cyclic heating/cooling, thus resulting in excellent thermal cycling resistance. Furthermore, the intensities of Si peaks increase with increasing Si content.

3.2. Mechanical properties

Noticeable differences concerning the stress–strain response during tensile testing are observed among the Al–Si alloys, as depicted in Fig. 3. It is seen that the tensile response becomes increasingly brittle as the Si content increases. The Al–22 wt.% Si and Al–27 wt.% Si alloys show pronounced plastic deformation, i.e., deviation from the linear elastic behavior. This deviation begins at around 20% of the ultimate tensile strength (UTS). Furthermore, the slope of the stress–strain curves becomes increasingly flatter until final failure [26]. The total strains to rupture for these alloys are comparatively high, whereas they display relatively lower UTS. For the Al–42 wt.% Si and Al–50 wt.% Si alloys, plastic deformation starts later (approximately 40% of the UTS). These samples undergo pronounced strain hardening until final failure, leading to the highest tensile strength but also clearly lower total strain compared to the alloys with low Si content. The presence of semi-continuous Si phase may contribute to the low ductility of the samples with high Si contents. According to the rule of mixture (ROM), the addition of more brittle Si phase significantly decreases the elongation to fracture. Another reason for this is that at high content of reinforcement, the distance between the hard phase decreases; thus, the dislocation movement is hindered. This is considered to be one of the most important factors in decreasing the elongation of this alloy.

Acceptable mechanical properties is another requirement for the application of Al–Si alloys in the electronic packaging industries to avoid damage under external pressure, shake and impact during the process of assembly and carriage. There is an obvious effect of Si content on the mechanical properties of the Al–Si alloys, as seen in Fig. 4. The values increase linearly with increasing Si content. Young's modulus primarily depends on the elastic properties and the corresponding volume fraction of reinforcement [26]; thus, it is expected to increase as the content of Si increases in the matrix. Neglecting the discrepancy of the reinforcement morphology and size, Young's modulus mainly depends on the content of Si phase for these alloys.

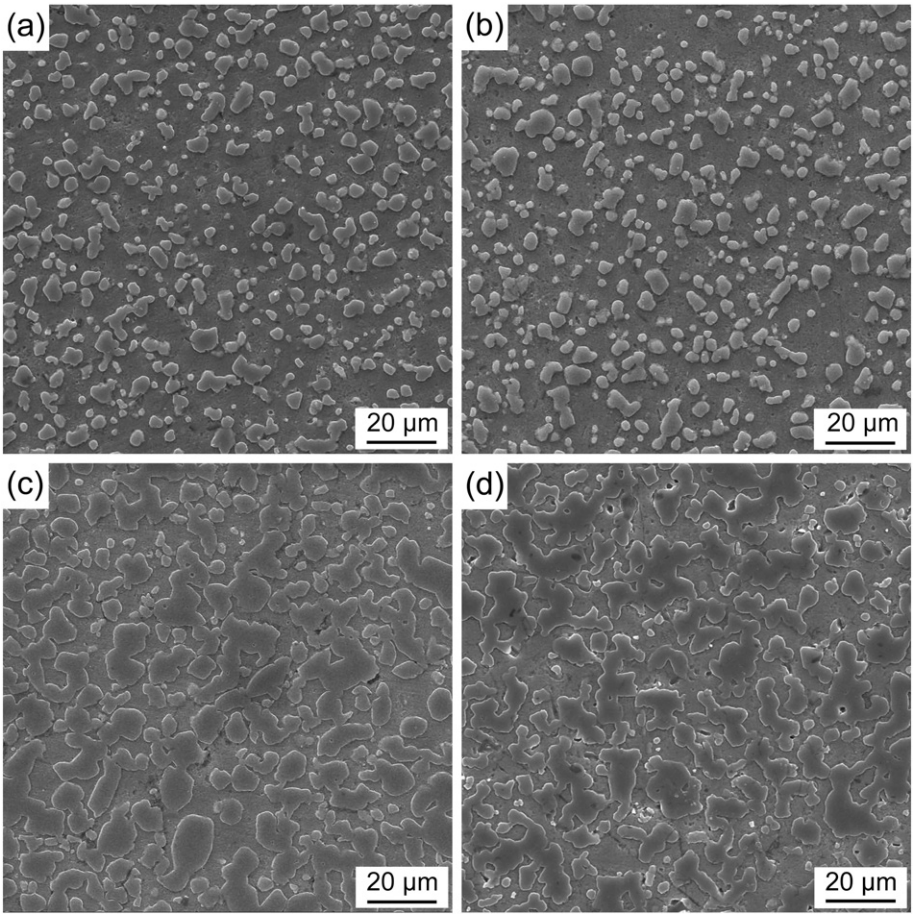

Fig. 1. Microstructures of the alloy samples: (a) Al–22 wt.% Si, (b) Al–27 wt.% Si, (c) Al–42 wt.% Si, and (d) Al–50 wt.% Si.

The effective tensile strength values are depicted in Fig. 4. The tensile strength of the alloys is clearly influenced by the Si content; the strength increases greatly as the Si content increases from 22 to 50 wt.%. It can be seen that the tensile strength increases from 148 to 196 MPa with increasing Si content. The reason is that Si particles prevent the movement of dislocations in the Al matrix through dispersion strengthening mechanism. Additionally, increasing the Si content also leads to a decrease in the distance among the Si particles. This phenomenon increases the hardness and the required tension for dislocations movement among the Si particles, leading to an increase in the strength.

The results of three-point bending tests as a function of Si content are also plotted in Fig. 4. Similarly, the bending strength is found to increase with increasing Si content. The Al–Si alloys yield a bending strength from 188 to 312 MPa. On the other hand, the bending strength (by about 66%) is more obviously influenced by the Si content than the tensile strength (by about 32%). This phenomenon should come from the characteristics of Si phase, such as size, morphology, and size distribution. Therefore, large deviation between tensile and bending strength occurs in the samples with high Si contents.

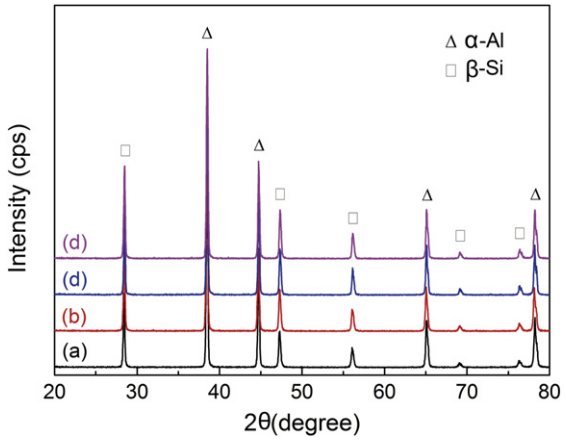

Fig. 2. XRD patterns of the alloy samples: (a) Al–22 wt.% Si, (b) Al–27 wt.% Si, (c) Al–42 wt.% Si, and (d) Al–50 wt.% Si.

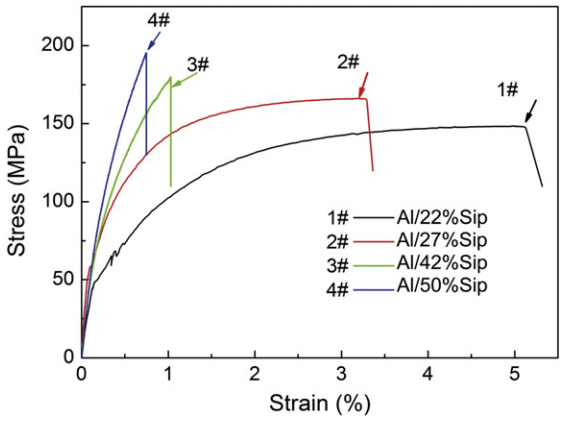

Fig. 3. Typical tensile stress curves of the Al–Si alloys prepared by hot pressing.

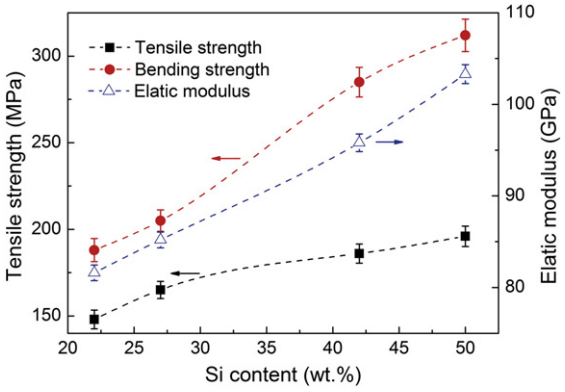

Fig. 4. Tensile strength, bending strength, and Young's modulus of the Al–Si alloys as a function of the Si content.

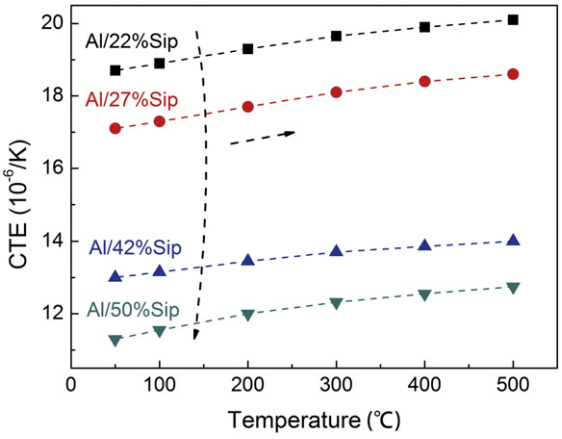

Fig. 5. Temperature dependence of CTE curves of the Al–Si alloys.

3.3. Physical properties

The measured densities of the Al–Si alloys are less than 2.7 g/cm^3, as illustrated in Table 1. By comparing the theoretical density obtained through the ROM, fully dense materials are achieved. It is worth noting that the density of such material is only about 80%, 30%, and 15% of the Al–SiCp composite, Kovar alloy, and W–Cu composite, respectively. This is desirable in the applications that require a low weight. This result indicates that the current hot pressing process with gas atomized alloy powder is a feasible method for fabricating the Al–Si alloys for thermal management applications.

Fig. 5 presents the CTE values with varying temperature for the Al–Si alloys investigated at 50–400 °C. It can be observed that, within the entire temperature range, increasing the Si content significantly reduces the CTE from 18.7 to 11.3 10^{-6}/K. Such a reduction in CTE is considered as a result of mixture rule and the intense restriction effect of Si reinforcement on the thermal expansion of the Al matrix.

Moreover, the CTE values increase linearly with increasing temperature but they show a relatively sluggish increase at high temperatures. This phenomenon has resulted from the combined effect of the solubility of Si in Al and the change of internal stress on the matrix when the temperature increases [23]. According to the Al–Si binary phase diagram, the concentration of Si in the Al rises as the temperature increases. In the Al matrix, increasing solid solubility of Si has a negative effect on the CTE because the lattice parameter of Al decreases with the increment of Si solubility, and the change in lattice parameter and macroscopic length counteract in the case of dilute solid [27]. Thus, the increasing rate of the CTE for Al–Si alloys decreases when the temperature increases beyond a certain point (about 250 °C). Another reason for the change of the CTE with temperature is the change of stress within the samples related to the temperature. A residual thermal stress will be generated in the sample cooled from the fabrication temperature due to the large difference in the CTE between the Si particles and the Al matrix [9]. Residual stress exhibits as compressive stress on the Si particle and tensile stress on the Al matrix. Thus, during heating from room temperature, the tensile stress on the matrix is relieved and the matrix is expanded, while at the same time it also helps the expansion of the matrix. When the tensile stress reduces to zero, a new compressive stress on the matrix is induced due to the CTE mismatch. This in turn results in a decrease in the CTE of the matrix. Although the level of stress on the Si particle is opposite the Al matrix, its effect on the CTE of the alloy can be ignored because of the large modulus and strength of Si phase. Thus, it is almost impossible for the stress to affect the CTE.

Several theoretical and numerical studies have provided expressions for the CTE of particulate composites based on various assumptions. In this work, the ROM, Turner, and Kerner models are used to model the temperature dependence behavior of the CTE of the Al–Si alloys. If the matrix modulus is much smaller than that of the reinforcement, the CTE is expressed by the ROM model [28].

$$\alpha = \alpha_m V_m + \alpha_p V_p, \tag{1}$$

where α is CTE, 10^{-6}/K; V is the volume fraction, vol.%; and the subscripts m and p refer to the matrix and particle, respectively.

The Turner model [29] assumes that the matrix and reinforcement are completely bonded, expand at the same rate, and the shear deformation is negligible. Moreover, it does not take the angularity and distribution of the reinforcement into consideration. The Turner model considers the uniform hydrostatic stresses and gives the CTE of a composite as

$$\alpha = \frac{\alpha_m V_m K_m + \alpha_p V_p K_p}{V_m K_m + V_p K_p}, \tag{2}$$

where K is the bulk modulus ($K = E/[3(1\text{-}2\upsilon)]$), GPa; E is the Young's modulus, GPa; and K_m and K_p stand for the bulk moduli of the matrix and the reinforcement.

Both the normal and shear stresses are taken into account in the Kerner model [30], and the CTE is expressed as

$$\alpha = \alpha_m V_m + \alpha_p V_p + \left(\frac{4G_m}{K}\right)\left[\frac{(K-K_p)(\alpha_m-\alpha_p)V_p}{4G_m + 3K_p}\right], \tag{3}$$

$$K = \left(\frac{V_m K_m}{3K_m + 4G_m} + \frac{V_p K_p}{3K_p + 4G_m}\right) \Big/ \left(\frac{V_m}{3K_m + 4G_m} + \frac{V_p}{3K_p + 4G_m}\right), \tag{4}$$

Table 1
Measured and theoretical density of the Al–Si alloys.

Materials	Theoretical density, g/cm^3	Measured density, g/cm^3	Relative density, %
Al/22 wt.% Sip	2.609	2.614	100.2
Al/27 wt.% Sip	2.589	2.586	99.9
Al/42 wt.% Sip	2.531	2.523	99.7
Al/50 wt.% Sip	2.501	2.496	99.8

Table 2
Physical properties of the Al and Si.

Material	ρ (g/cm^3)	E (GPa)	G (GPa)	K (GPa)	CTE (10^{-6}/K)	υ
Al	2.70	69.2	26.0	67.8	22.6	0.33
Si	2.33	163	66.8	97.0	2.5	0.22

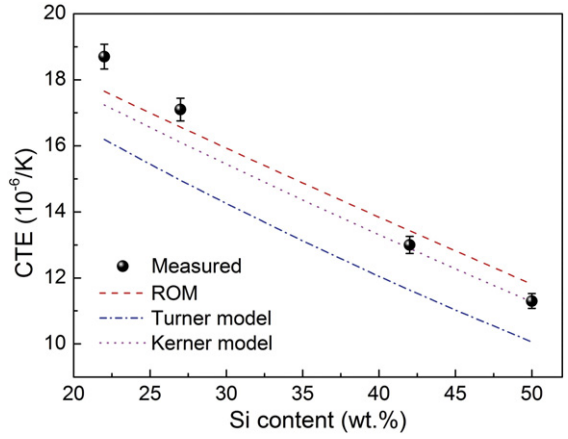

Fig. 6. Comparison of measured and theoretical CTE of the Al–Si alloys with various Si contents.

where G is the shear modulus ($G = E/[2(1+\upsilon)]$), GPa. The material parameters used in the calculations are given in Table 2.

Fig. 6 displays the comparison between the measured and calculated CTE of the Al–Si alloys. It can be seen that the theoretical values based on the Kerner model agree well with the experimental values of the alloys with high Si contents, but deviate from the ROM and Turner models. This may be attributed to the fact that the normal and shear stress are included in the Kerner model, while the ROM and Turner models could not describe the complicated internal stresses inside the alloys. However, the measured values of the alloys with low Si contents are significantly higher than the theoretical values. The reason should come from the fact that the theoretical models is feasible for AMCs with high reinforcement contents, while the volume fraction of Si in the Al–22 wt.% Si and Al–27 wt.% Si alloys are less than 30%. Additionally, the Si phase in the two samples with nearly spherical shape that could not effectively suppress the expansion of Al matrix may also result in the high CTE.

Fig. 7 shows the thermal conductivity of the hot pressed Al–Si alloys. It can be seen that the thermal conductivity decreases from 187 to 145 W/m K with increasing Si content due to the lower thermal conductivity of Si (148 W/m K) in contrast with Al (238 W/m K). The thermal conductivity of Al–50 wt.% Si alloy is higher than that fabricated at 520 °C for 120 min (~130 W/m K) [31] due to the high consolidation temperature and the use of high purity Al and Si. This value is also higher than that of Al–55 vol.% SiC composite prepared by pressureless infiltration (~125 W/m K) [27,32]. In the present work, the high thermal conductivity of the alloys is attributed to their highly dense and uniform microstructures. The thermal conductivity is also influenced by the defects, such as micro-pores, in the material. The pores in the material will decrease the overall thermal conductivity because the air is a poor thermal conductor. The hot pressing of the pre-alloyed powder leads to a dense microstructure which improves the thermal conduction capability of the alloys. Furthermore, the thermal conductivity/density ratio of Al–50 wt.% Si alloy (58.4) is several times larger than those of the traditional thermal management materials, especially the W–Cu and Mo–Cu composites (~13.8).

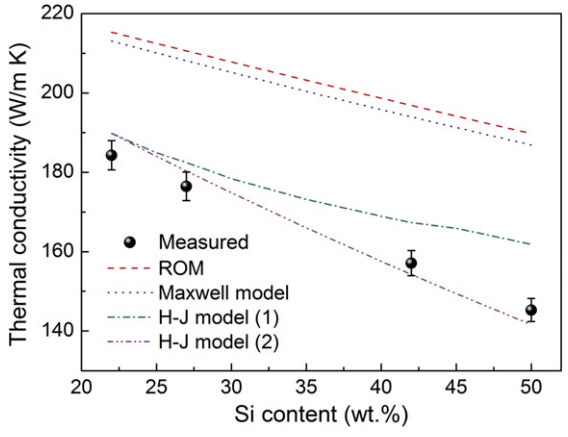

Fig. 7. Variation in thermal conductivity of the Al–Si alloys against the Si content.

The thermal conductivity of composites depends on the thermal conductivity of each component, volume fraction, distribution, and size of reinforcement, density, and interfacial bonding strength between the matrix and reinforcement. Researchers have constructed many theoretical models to describe the impact of these factors on the thermal conductivity of composites. Among those models, the Hasselman–Johnson (H–J) model [33] is known as the most accurate since it takes into account the combined effects of particle size, volume fraction, and interfacial thermal resistance. The H–J model assumes that the thermal contact between matrix and reinforcement is not perfect and, thus, the interface acts as an effective heat flow barrier, and this model is described as

$$\lambda = \lambda_m \cdot \frac{2V_p\left(\frac{\lambda_p}{\lambda_m} - \frac{R_c \cdot \lambda_p}{r} - 1\right) + \frac{\lambda_p}{\lambda_m} + 2\frac{R_c \cdot \lambda_p}{r} + 2}{V_p\left(1 - \frac{\lambda_p}{\lambda_m} + \frac{R_c \cdot \lambda_p}{r}\right) + \frac{\lambda_p}{\lambda_m} + 2\frac{R_c \cdot \lambda_p}{r} + 2}, \tag{5}$$

where λ is the thermal conductivity, W/m K; r is the radius of the reinforcement, m; R is the interfacial thermal resistance, m^2 K/W. The interfacial thermal resistance is correlated the temperature drop across an interface to the interfacial heat flux, which depends on the solid adjacent to the boundary and the quality of the interfaces themselves.

The interfacial thermal resistance can be estimated by a simple Debye model in terms of the Acoustic Mismatch model (AMM) [34–36]. It is expressed by

$$R = \frac{2\left(\rho_m D_m + \rho_p D_p\right)^2}{C_m \cdot \rho_m^2 \cdot D_m^2 \cdot \rho_p \cdot D_p}\left(\frac{D_p}{D_m}\right)^2, \tag{6}$$

where ρ is the density, kg/m^3; C is the specific heat, J/kg K; D is the Debye velocity, m/s. The value of D can be estimated by [37]

$$D = \sqrt{G/\rho}. \tag{7}$$

For comparison, the ROM and Maxwell models are also used in the calculation, and the results are present in Fig. 7. The Maxwell model assumes a perfect interface bonding in the case of H–J model. The material parameters for calculation are provided in Table 2. It can be seen that the predicted values using the ROM and Maxwell models are much higher than the experimental values. This is reasonable because the Maxwell model is adopted without consideration of the thermal resistance (3.4×10^{-9} m^2 K/W) generated at the matrix-reinforcement boundary and the non-spheroidicity of the reinforcement. Additionally, the surface roughness and oxide layer on the Si particles also increase the thermal boundary resistance and then the thermal conductivity of the Al–Si alloys [38].

The H–J model (1) takes the size of reinforcement into account and, therefore, the predicted values are in good agreement with the experimental values for the alloys with low Si contents; however, these values are not consistent with those for the alloys with high Si contents. In contrast, neglecting the difference in size of reinforcement, the results based on the H–J model shows good agreement with all the experimental results (H–J model (2)). The size, shape, and spheroidicity of

reinforcement have great influence on the thermal conductivity of composites [4,37,39]. The deviation between the predicted values indicates that the size of reinforcement has a significant effect on the thermal conductivity of particulate composites. Although it is favorable for the thermal conductivity with the addition of large reinforcement, the decrease in the thermal conductivity of the Al–42 wt.% Si and Al–50 wt.% Si alloys should be attributed to the evolution of Si phase morphology, as shown in Fig. 1, where the Si phase in these samples shows continuous network but it displays near spherical shape in the other two samples with lower Si contents. Meanwhile, large amount of oxide (from 870 to 1167 ppm) presents in the Al–Si alloys with high Si contents due to the high melting temperature during atomization. The evolution of Si phase with high Si content is different to the traditionally particulate AMCs and a shape factor introduced for the H–J model may be demanded for the present alloys [39]. Additionally, such result may indicate that there is still room for further enhancement in the thermal conductivity of the Al–Si alloys by optimizing the processing parameters.

3.4. Fractography

The tensile fracture surfaces of the investigated alloys with different Si contents are shown in Fig. 8. It can be seen that the samples with low Si contents exhibit ductile behavior with visible dimples (Fig. 8a and b). While, no visible macro-ductility fracture is observed in the samples with high Si contents (Fig. c and d). It is also noted that the fracture surface of the crack source is more flatten than the nearby area. Further observation indicates that the Al matrix fails via ductile rupture, especially in the Al–22 wt.% Si and Al–27 wt.% Si alloys, and the Si phase fails by cleavage fracture. However, shear-type plastic deformation of the Al matrix is less evident for the samples with higher Si contents, as seen in Fig. 8c and d. The loss of ductility is ascribed to the higher content of brittle Si phase. In addition, no visible interfacial debonding is found in all samples, indicating the excellent interfacial bonding strength between the Al matrix and Si phase. The probable fracture mechanism of the Al–Si alloys is described in the form of brittle fracture of the Si phase followed by tearing up of the surrounding Al matrix.

4. Conclusions

In this work, Al–Si alloys were prepared by hot pressing of the gas atomized Al–Si alloy powder. The effects of Si content on the microstructure, mechanical and physical properties, and fracture mechanism were investigated, and the following conclusions were obtained.

1) Dense Al–Si alloys with the Si content of 22–50 wt.% could be obtained by hot pressing of the gas atomized alloy powder, of which the relative densities are higher than 99%. The alloys show a pore-free microstructure with homogeneously dispersed fine Si phase in the Al matrix. The alloys are composed of the α-Al and β-Si phases without any interfacial reactions.
2) The tensile response of the Al–Si alloys becomes increasingly brittle as the Si content increases. Additionally, the tensile strength, bending strength, and Young's modulus of the alloys are significantly improved with increasing Si content.
3) The CTE and thermal conductivity of the Al–Si alloys decrease as the Si content increases. The Kerner model and H–J model could be used to predict the CTE and thermal conductivity of the alloys, even though some discrepancy still presented. The average CTE and thermal conductivity of the Al–Si alloys containing 22–50 wt.% Si are

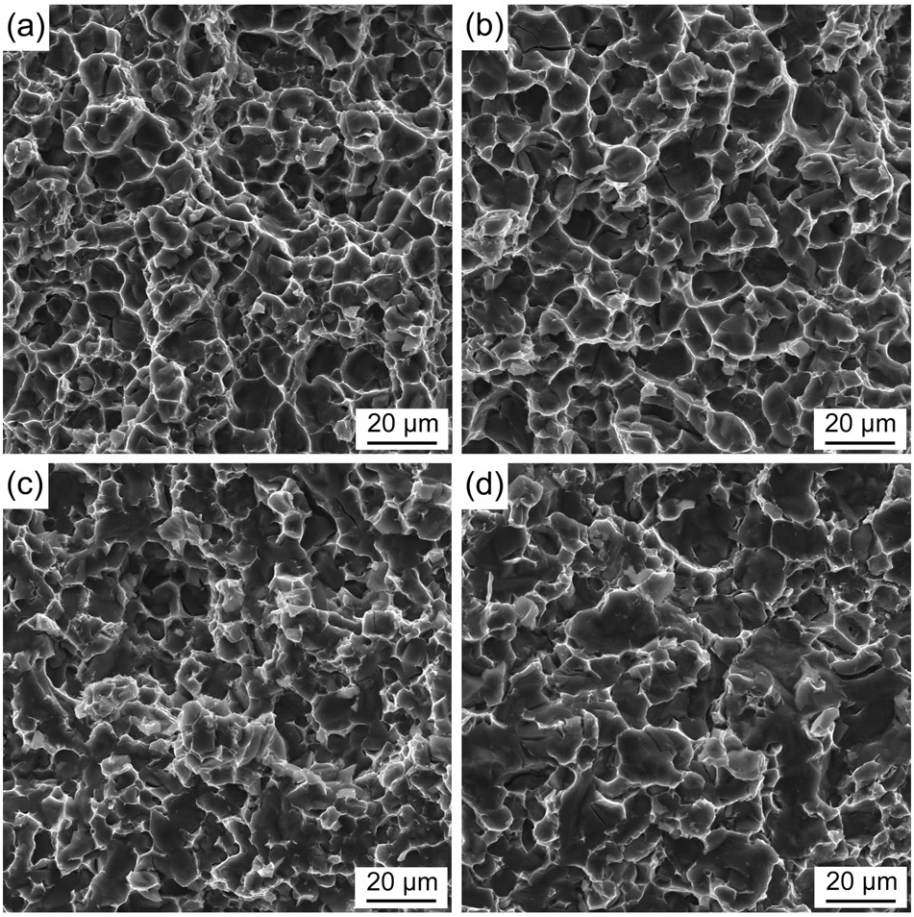

Fig. 8. Tensile fracture surfaces of the Al–Si alloys with Si content of (a) 22 wt.%, (b) 27 wt.%, (c) 42% wt.%, and (d) 50% wt.%.

18.7–11.3 10^{-6}/K and 184–145 W/m K, respectively, thus they are desirable for the applications in electronic packaging.

4) The Al–Si alloys exhibit brittle fracture features, especially the samples with high Si contents. No visible interfacial debonding is found in all broken tensile samples.

Acknowledgment

The authors would like to thank for the financial support from the National Key Fundamental Research Project of China (JPPT-125-14).

References

[1] J.H. Yu, C.B. Wang, Q. Shen, L.M. Zhang, Preparation and properties of Sip/Al composites by spark plasma sintering, Mater. Des. 41 (2012) 198–202.
[2] J. Cho, K.E. Goodson, Thermal transport: cool electronics, Nat. Mater. 14 (2015) 136–137.
[3] J.M. Molina, J. Narciso, L. Weber, A. Mortensen, E. Louis, Thermal conductivity of Al–SiC composites with monomodal and bimodal particle size distribution, Mater. Sci. Eng. A 480 (2008) 483–488.
[4] D.P.H. Hasselman, K.Y. Donaldson, Effect of reinforcement particle size on the thermal conductivity of a particulate silicon carbide-reinforced aluminium-matrix composite, J. Am. Ceram. Soc. 75 (1992) 3137–3140.
[5] P.W. Ruch, O. Beffort, S. Kleiner, L. Weber, P.J. Uggowitzer, Selective interfacial bonding in Al(Si)–diamond composites and its effect on thermal conductivity, Compos. Sci. Technol. 66 (2006) 2677–2685.
[6] L. Weber, J. Dorn, A. Mortensen, On the electrical conductivity of metal matrix composites containing high volume fractions of non-conducting inclusions, Acta Mater. 51 (2003) 3199–3211.
[7] A. Miserez, R. Müller, A. Mortensen, Increasing the strength/toughness combination of high volume fraction particulate metal matrix composites using an Al–Ag matrix alloy, Adv. Eng. Mater. 8 (2006) 56–62.
[8] Y.Q. Liu, S.H. Wei, J.Z. Fan, Z.L. Ma, T. Zuo, Mechanical properties of a low-thermal-expansion aluminum/silicon composite produced by powder metallurgy, J. Mater. Sci. Technol. 30 (2014) 417–422.
[9] Y. Jia, F. Cao, S. Scudino, P. Ma, H. Li, L. Yu, et al., Microstructure and thermal expansion behavior of spray-deposited Al–50Si, Mater. Des. 57 (2014) 585–591.
[10] K. Hummert, B. Commandeur, A. Leatham, A. Ogilvy, W. Hunt Jr., High performance, low cost aluminium alloys manufactured by spray forming, Proceedings of the Powder Metallurgy Aluminum & Light Alloys for Automotive Applications Conference (USA), Metal Powder Industries Federation 1998, pp. 107–114.
[11] H. Neubing, J. Gradl, H. Danninger, Sintering and microstructure of Al–Si P/M components, Adv. Powder Metall. Part. Mater. (2002) 13–128.
[12] W. Yu, J.K. Yu, Silicon dissolution and interfacial characteristics in Si/Al composites fabricated by gas pressure infiltration, Mater. Chem. Phys. 139 (2013) 783–788.
[13] Z. Cai, R. Wang, C. Zhang, C. Peng, L. Wang, Microstructure and properties of Al/Sip composites for thermal management applications, J. Mater. Sci. Mater. Electron. 26 (2015) 4234–4240.
[14] Y. Chen, D.D. Chung, Silicon–aluminum network composites fabricated by liquid metal infiltration, J. Mater. Sci. 29 (1994) 6069–6075.
[15] Z. Xiu, G. Wu, Q. Zhang, M. Song, S. Tian, Microstructure and electric properties of Sip/Al composites for electronic packaging applications, Trans. Nonferrous Metals Soc. China 17 (2007) 1034–1038.
[16] S.C. Hogg, A. Lambourne, A. Ogilvy, P.S. Grant, Microstructural characterisation of spray formed Si–30Al for thermal management applications, Scr. Mater. 55 (2006) 111–114.
[17] Q. Jia, J. Liu, Y. Li, W. Wang, Microstructure and properties of electronic packaging box with high silicon aluminum-base alloy by semi-solid thixoforming, Trans. Nonferrous Metals Soc. China 23 (2013) 80–85.
[18] C.W. Chien, S.L. Lee, J.C. Lin, Processing and properties of high volume fraction aluminium/silicon composites, Mater. Sci. Technol. 19 (2003) 1231–1234.
[19] B. Ogel, R. Gurbuz, Microstructural characterization and tensile properties of hot pressed Al–SiC composites prepared from pure Al and Cu powders, Mater. Sci. Eng. A 301 (2001) 213–220.
[20] Q. Zhang, B.L. Xiao, Z.Y. Liu, Z.Y. Ma, Microstructure evolution and elemental diffusion of SiCp/Al–Cu–Mg composites prepared from elemental powder during hot pressing, J. Mater. Sci. 46 (2011) 6783–6793.
[21] A. Canakci, T. Varol, Microstructure and properties of AA7075/Al–SiC composites fabricated using powder metallurgy and hot pressing, Powder Technol. 268 (2014) 72–79.
[22] Q. Zhang, L. Jiang, G. Wu, Microstructure and thermo-physical properties of a SiC/pure-Al composite for electronic packaging, J. Mater. Sci. Mater. Electron. 25 (2013) 604–608.
[23] Q. Zhang, G. Wu, L. Jiang, G. Chen, Thermal expansion and dimensional stability of Al–Si matrix composite reinforced with high content SiC, Mater. Chem. Phys. 82 (2003) 780–785.
[24] J.V. Goñi, J.M. Rodriguez-Ibabe, J.J. Urcola, Strength and toughness of semi-solid processed hypereutectic Al/Si alloys, Scr. Mater. 34 (1996) 483–489.
[25] Z. Cai, R. Wang, C. Zhang, C. Peng, Y. Feng, L. Wang, Thermal cycling reliability of Al/50Sip composite for thermal management in electronic packaging, J. Mater. Sci. Mater. Electron. 26 (2015) 4894–4901.
[26] O. Beffort, S. Long, C. Cayron, J. Kuebler, P.-A. Buffat, Alloying effects on microstructure and mechanical properties of high volume fraction SiC-particle reinforced Al-MMCs made by squeeze casting infiltration, Compos. Sci. Technol. 67 (2007) 737–745.
[27] S. Ren, X. He, X. Qu, I.S. Humail, Y. Li, Effect of Si addition to Al–8Mg alloy on the microstructure and thermo-physical properties of SiCp/Al composites prepared by pressureless infiltration, Mater. Sci. Eng. B 138 (2007) 263–270.
[28] A.L. Geiger, M. Jackson, Low expansion MMCs boost avionics, Mater. Sci. Forum 7 (1989) 23–29.
[29] P.S. Turner, Thermal expansion stresses in reinforced plastics, J. Res. NBS 37 (1946) 239–244.
[30] E.H. Kerner, The elastic and thermo-elastic properties of composite media, Proc. Phys. Soc. B 69 (1956) 808–813.
[31] G. Mi, C. Li, K. Wang, L. Chen, Microstructure and properties of 50Si50Al alloy fabricated by HPS process using overspray powders, Mater. Res. Innov. 17 (2013) 182–185.
[32] Q. Wang, F. Min, J. Zhu, Microstructure and thermo-mechanical properties of SiCp/Al composites prepared by pressureless infiltration, J. Mater. Sci. Mater. Electron. 24 (2012) 1937–1940.
[33] D.P.H. Hasselman, L.F. Johnson, Effective thermal conductivity of composites with interfacial thermal barrier resistance, J. Compos. Mater. 21 (1987) 508–515.
[34] E.T. Swartz, R.O. Pohl, Thermal boundary resistance, Rev. Mod. Phys. 61 (1989) 605–668.
[35] S. Ren, X. Shen, C. Guo, N. Liu, J. Zang, X. He, et al., Effect of coating on the microstructure and thermal conductivities of diamond–Cu composites prepared by powder metallurgy, Compos. Sci. Technol. 71 (2011) 1550–1555.
[36] A.G. Every, Y. Tzou, D.P.H. Hasselman, R. Raj, The effect of particle size on the thermal conductivity of ZnS/diamond composites, Acta Metall. Mater. 40 (1992) 123–129.
[37] J. Wang, X.-S. Yi, Effects of interfacial thermal barrier resistance and particle shape and size on the thermal conductivity of AlN/PI composites, Compos. Sci. Technol. 64 (2004) 1623–1628.
[38] P.E. Hopkins, L.M. Phinney, J.R. Serrano, T.E. Beechem, Effects of surface roughness and oxide layer on the thermal boundary conductance at aluminum/silicon interfaces, Phys. Rev. B 82 (2010).
[39] S.V. Kidalov, F.M. Shakhov, Thermal conductivity of diamond composites, Materials 2 (2009) 2467–2495.